A Bacterium That Can Grow by Using Arsenic Instead of Phosphorus

Felisa Wolfe-Simon,[1,2]* Jodi Switzer Blum,[2] Thomas R. Kulp,[2] Gwyneth W. Gordon,[3] Shelley E. Hoeft,[2] Jennifer Pett-Ridge,[4] John F. Stolz,[5] Samuel M. Webb,[6] Peter K. Weber,[4] Paul C. W. Davies,[1,7] Ariel D. Anbar,[1,3,8] Ronald S. Oremland[2]

Life is mostly composed of the elements carbon, hydrogen, nitrogen, oxygen, sulfur, and phosphorus. Although these six elements make up nucleic acids, proteins, and lipids and thus the bulk of living matter, it is theoretically possible that some other elements in the periodic table could serve the same functions. Here, we describe a bacterium, strain GFAJ-1 of the Halomonadaceae, isolated from Mono Lake, California, that is able to substitute arsenic for phosphorus to sustain its growth. Our data show evidence for arsenate in macromolecules that normally contain phosphate, most notably nucleic acids and proteins. Exchange of one of the major bio-elements may have profound evolutionary and geochemical importance.

Biological dependence on the six major nutrient elements carbon, hydrogen, nitrogen, oxygen, sulfur, and phosphorus (P) is complemented by a selected array of other elements, usually metals or metalloids present in trace quantities that serve critical cellular functions, such as enzyme co-factors (1). There are many cases of these trace elements substituting for one another. A few examples include the substitution of tungsten for molybdenum and cadmium for zinc in some enzyme families (2, 3) and copper for iron as an oxygen-carrier in some arthropods and mollusks (4). In these examples and others, the trace elements that interchange share chemical similarities that facilitate the swap. However, there are no prior reports of substitutions for any of the six major elements essential for life. Here, we present evidence that arsenic can substitute for phosphorus in the biomolecules of a naturally occurring bacterium.

Arsenic (As) is a chemical analog of P, which lies directly below P on the periodic table. Arsenic possesses a similar atomic radius, as well as near identical electronegativity to P (5). The most common form of P in biology is phosphate (PO_4^{3-}), which behaves similarly to arsenate (AsO_4^{3-}) over the range of biologically relevant pH and redox gradients (6). The physicochemical similarity between AsO_4^{3-} and PO_4^{3-} contributes to the biological toxicity of AsO_4^{3-} because metabolic pathways intended for PO_4^{3-} cannot distinguish between the two molecules (7) and AsO_4^{3-} may

be incorporated into some early steps in the pathways [(6) and references therein]. However, it is thought that downstream metabolic processes are generally not compatible with As-incorporating molecules because of differences in the reactivities of P and As compounds (8). These downstream biochemical pathways may require the more chemically stable P-based metabolites; the lifetimes of more easily hydrolyzed As-bearing analogs are thought to be too short. However, given the similarities of As and P—and by analogy with trace element substitutions—we hypothesized that AsO_4^{3-} could specifically substitute for PO_4^{3-} in an organism possessing mechanisms to cope with the inherent instability of AsO_4^{3-} compounds (6). Here, we experimentally tested this hypothesis by using AsO_4^{3-}, combined with no added PO_4^{3-}, to select for and isolate a microbe capable of accomplishing this substitution.

Geomicrobiology of GFAJ-1. Mono Lake, located in eastern California, is a hypersaline and alkaline water body with high dissolved arsenic concentrations [200 µM on average (9)]. We used lake sediments as inocula into an aerobic defined artificial medium at pH 9.8 (10, 11) containing 10 mM glucose, vitamins, and trace metals but no added PO_4^{3-} or any additional complex organic supplements (such as yeast extract or peptone), with a regimen of increasing AsO_4^{3-} additions initially spanning the range from 100 µM to 5 mM. These enrichments were taken through many decimal-dilution transfers, greatly reducing any potential carryover of autochthonous phosphorus
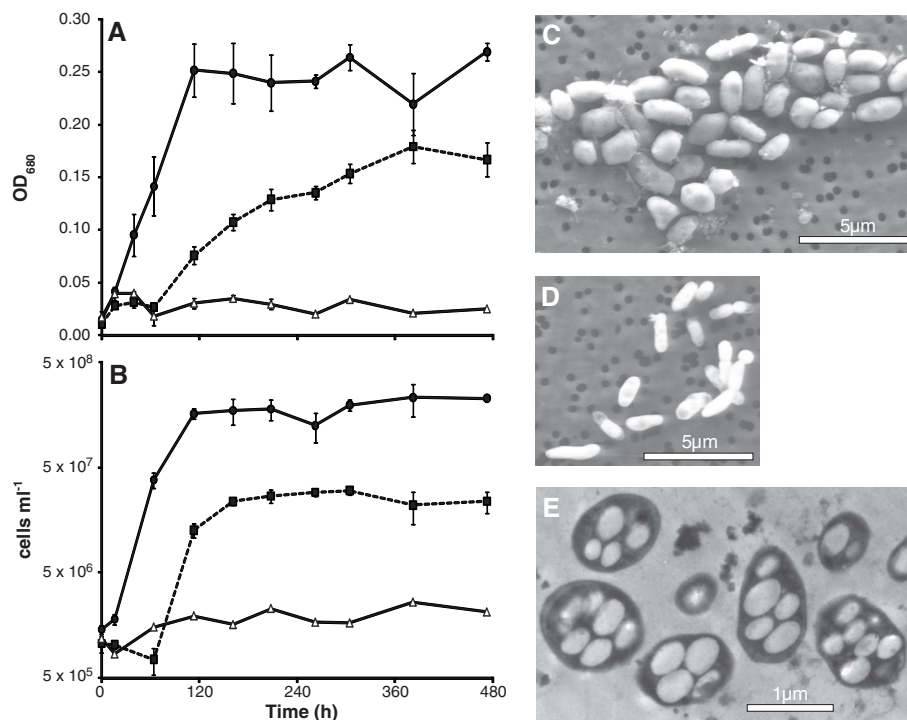

Fig. 1. Growth and electron microscopy of strain GFAJ-1. (**A** and **B**) Growth curves of GFAJ-1 grown on the defined synthetic medium amended with either 1.5 mM PO_4^{3-} (solid circles), 40 mM AsO_4^{3-} (solid squares), or neither PO_4^{3-} nor AsO_4^{3-} (open triangles). Cell growth was monitored both by an increase in (A) optical density and (B) cell numbers of the cultures. Symbols represent the mean ± SD of (A) $n = 6$ experimental and $n = 2$ controls and (B) $n = 3$ experimental and $n = 1$ control. This was a single experiment with six replicates; however, material was conserved to extend the duration of the experiment to allow material for cell-counting samples. (**C** and **D**) Scanning electron micrographs of strain GFAJ-1 under two conditions, (C) +As/–P and (D) –As/+P. (**E**) Transmission electron micrography of +As/–P GFAJ-1 showed internal vacuole-like structures. Scale bars are as indicated in the figure (11).

[1]NASA Astrobiology Institute, USA. [2]U.S. Geological Survey, Menlo Park, CA 94025, USA. [3]School of Earth and Space Exploration, Arizona State University, Tempe, AZ 85287, USA. [4]Lawrence Livermore National Laboratory, Livermore, CA 94551, USA. [5]Department of Biological Sciences, Duquesne University, Pittsburgh, PA 15282, USA. [6]Stanford Synchrotron Radiation Lightsource, Menlo Park, CA 94025, USA. [7]BEYOND: Center for Fundamental Concepts in Science, Arizona State University, Tempe, AZ 85287, USA. [8]Department of Chemistry and Biochemistry, Arizona State University, Tempe, AZ 85287, USA.

*To whom correspondence should be addressed. E-mail: felisawolfesimon@gmail.com

(11). The background PO_4^{3-} in the medium was 3.1 ($\pm$ 0.3) μM on average, with or without added AsO_4^{3-}, coming from trace impurities in the major salts (table S1) (11). The sixth transfer of the 5 mM AsO_4^{3-} (no added PO_4^{3-}) condition was closely monitored and demonstrated an approximate growth rate (μ) of 0.1 day^{-1}. After 10^{-7} dilutions, we used the 5 mM AsO_4^{3-} enrichment to inoculate an agar plate that contained the same chemical composition as the artificial medium. An isolated colony was picked from the agar plates and reintroduced into an artificial liquid medium with no added PO_4^{3-}, where we then progressively increased the AsO_4^{3-} concentration to determine the optimal level for growth. Currently, this isolate—strain GFAJ-1 identified by 16S ribosomal RNA sequence phylogeny as a member of the Halomonadaceae family of Gammaproteobacteria (fig. S1) (11)—is maintained aerobically with 40 mM AsO_4^{3-}, 10 mM glucose, and no added PO_4^{3-} (+As/–P condition). Members of this family have been previously shown to accumulate intracellular As (12).

GFAJ-1 grew at an average μ_{max} of 0.53 day^{-1} under +As/–P, increasing by over 20-fold in cell numbers after 6 days. It also grew faster and more extensively with the addition of 1.5 mM PO_4^{3-} (–As/+P, μ_{max} of 0.86 day^{-1}) (Fig. 1, A and B). However, when neither AsO_4^{3-} nor PO_4^{3-} was added no growth was observed (Fig. 1, A and B). We include both optical density and direct cell counts to unambiguously demonstrate growth using two independent methods. Cells grown under +As/–P were oblong and approximately 2 by 1 μm when imaged by means of scanning electron microscopy (Fig. 1C) (11). When grown under +As/–P conditions, GFAJ-1 cells had more than 1.5-fold greater intracellular volume ($\approx$2.5 $\pm$ 0.4 μm^3) as compared with that of –As/+P ($\approx$1.5 $\pm$ 0.5 μm^3) (Fig. 1D) (11). Transmission electron microscopy revealed large vacuole-like regions in +As/–P–grown cells that may account for this increase in size (Fig. 1E). These experiments demonstrated AsO_4^{3-}-dependent growth, morphological differences in GFAJ-1 driven by AsO_4^{3-} in the growth medium, and that the level of PO_4^{3-} impurities in the medium was insufficient to elicit growth in the control (–As/–P).

Cellular stoichiometry and elemental distribution. To determine whether GFAJ-1 was taking up AsO_4^{3-} from the medium, we measured the intracellular As content by means of inductively coupled plasma mass spectrometry (ICP-MS) (11). In +As/–P–grown cells, the mean intracellular As was 0.19 $\pm$ 0.25% by dry weight (Table 1), whereas the cells contained only 0.019 +/– 0.009 P by dry weight. This P was presumably scavenged from trace PO_4^{3-} impurities in the reagents and not likely due to carryover, given our enrichment and isolation strategy (11). Moreover, when grown +As/–P this intracellular P is 96.5% less than our measured P values for this microbe when grown –As/+P and far below the 1 to 3% P by dry weight required to support growth in a typical heterotrophic bacterium (13). In contrast, GFAJ-1 cells grown under –As/+P conditions had a mean P content of 0.54 $\pm$ 0.21% by dry weight. There was variation in the total As content of the +As/–P cells, which is possibly a result of collection during stationary phase and losses during the repeated centrifugations and washing cycles because of the potential instability of the cellular structures given their swollen state (Fig. 2, C and E). In contrast, the integrity of the –As/+P cells appeared robust (Fig. 2D), and thus intracellular P measured for these cells probably reflects their content. However, the low total intracellular P in +As/–P cells was consistently far below the quantity needed to support growth, suggesting that these low values are correct despite variation in data from the +As/–P cells. Low intracellular P in concert with high intracellular As was further confirmed through high-resolution secondary ion mass spectrometry and x-ray analyses, as discussed below.

We used radiolabeled $^{73}AsO_4^{3-}$ to obtain more specific information about the intracellular distribution of arsenic (11). We observed intracellular arsenic in protein, metabolite, lipid, and nucleic acid cellular fractions (Table 2). Stationary phase cells incorporated approximately $\frac{1}{10}$ of the total intracellular $^{73}AsO_4^{3-}$ label into nucleic acids but more than three quarters of the $^{73}AsO_4^{3-}$ into the phenol extracted "protein" fraction, with a small fraction going into lipids. We caution that the large "protein" fraction is probably an overestimate because this extraction step likely contains numerous small, non-proteinaceous metabolites as well. To determine whether this distribution pattern reflected a use of AsO_4^{3-} in place of PO_4^{3-} in DNA, we estimated the average sequenced bacterial genome to be 3.8 megabase pairs (Mbp), which would contain approximately 7.5 $\times$ 10^6 atoms or 12.5 $\times$ 10^{-18} moles of P. Assuming one complete genome per cell, this would equal 0.39 fg of P in the genome. Using ICP-MS, we measured about 9.0 fg P per cell in the –As/+P condition, which implies that only ~4% of total intracellular P is associated with the genome. Because these cells were harvested in stationary phase (11), the fraction of P associated with RNA is likely small (14). Hence, roughly 96% of P is presumably distributed between the "lipid" and "protein" fractions. If AsO_4^{3-} is substituting for PO_4^{3-} in DNA, then we can assume that roughly the same fraction of the total intracellular

Table 1. Bulk intracellular elemental profile of strain GFAJ-1. Cells were grown and prepared with trace metal clean techniques (11). Numbers in parentheses indicate replicate samples analyzed. As:P ratios were calculated based on all samples analyzed (11). Units are percent dry weight.

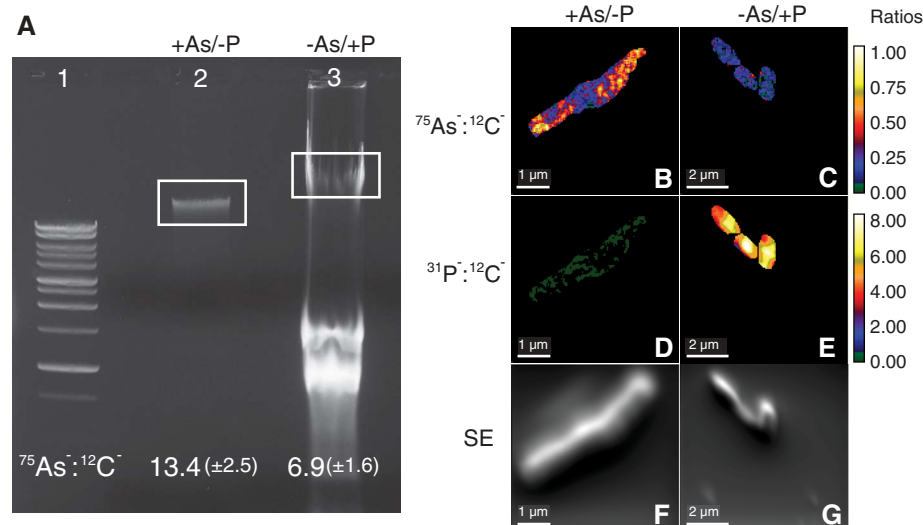| Condition	As	P	As:P
+As/–P (8)	0.19 $\pm$ 0.25	0.019 $\pm$ 0.009	7.3
–As/+P (4)	0.001 $\pm$ 0.0005	0.54 $\pm$ 0.21	0.002

Fig. 2. NanoSIMS analyses of GFAJ-1: extracted DNA and whole-cells elemental ratio maps. (**A**) Agarose gel loaded with DNA/RNA extracted from GFAJ-1 grown (lane 2) +As/–P and (lane 3) –As/+P as compared with (lane 1) a DNA standard. Genomic bands were excised as indicated and analyzed with NanoSIMS. Ion ratios of $^{75}As^-$:$^{12}C^-$ of excised gel bands are indicated below with 2σ error shown (all values multiplied by 10^{-6}). (**B** to **G**) NanoSIMS images of whole GFAJ-1 cells grown either [(B), (D), and (F)] +As/–P or [(C), (E), and (G)] –As/+P. Shown are the ion ratios of [(B) and (C)] $^{75}As^-$:$^{12}C^-$, [(D) and (E)] $^{31}P^-$:$^{12}C^-$, and [(F) and (G)] secondary electron (SE). Ratios in (B) and (C) are multiplied by 10^{-4} and in (D) and (E) are multiplied by 10^{-3}. The color bars indicate measured elemental ratios on a log scale as indicated. Length scale is as indicated on images; images contain equivalent pixel density (11).

AsO_4^{3-} would reflect a similar distribution to our estimated PO_4^{3-} distribution. The distribution of intracellular $^{73}AsO_4^{3-}$ in our experiments was consistent with these estimates. If AsO_4^{3-} is fulfilling the biological role of PO_4^{3-}, then AsO_4^{3-} should act in many analogous biochemical roles, including DNA, protein phosphorylation, small molecular weight metabolites [such as arsenylated analogs of the reduced form of nicotinamide adenine dinucleotide phosphate (NADH), adenosine triphosphate (ATP), and intermediates like glucose and acetyl–coenzyme A (acetyl-CoA)], and phospholipids.

Our data suggested that As was present in a number of biomolecules, and in particular we sought to confirm the presence of As in the DNA fraction. Initially, we measured traces of As with ICP-MS analysis of extracted nucleic acid and protein/metabolite fractions from +As/–P–grown cells (table S1) (11). We then used high-resolution secondary ion mass spectrometry (NanoSIMS) to identify As in extracted, gel-isolated genomic DNA (Fig. 2A). These data showed that DNA from +As/–P cells had elevated As and low P relative to DNA from the –As/+P cells. NanoSIMS analysis of the DNA showed that the As:P ratio on an atom-per-atom basis was significantly higher in the +As/–P versus –As/+P grown cells ($P = 0.02$) (Fig. 2A and table S2) (11). Whether expressed as an ion ratio relative to C ($^{75}As^-$:$^{12}C^-$), (Fig. 2A) or $^{31}P^-$:$^{12}C^-$ (table S2) (11), or normalized by relative ion yield and expressed as a concentration in parts per billion (table S2) (11), we saw a similarly consistent trend, with significantly higher As in the +As/–P DNA ($P = 0.03$) and higher P in the –As/+P DNA ($P = 0.0003$). In both cases, the nonamended element concentration was equal or less than background levels. These measurements therefore specifically demonstrated that the purified DNA extracted from +As/–P cells contained As. Our NanoSIMS analyses, combined with the evidence for intracellular arsenic by ICP-MS and our radiolabeled $^{73}AsO_4^{3-}$ experiments, indicated that intracellular AsO_4^{3-} was incorporated into key biomolecules, specifically DNA.

Characterization of the intracellular arsenic chemical environment. We next used synchrotron x-ray studies to determine the speciation and chemical environment of the intracellular arsenic (11). Micro–x-ray absorption near-edge spectroscopy (μXANES) of +As/–P–grown cells exhibited an absorption edge characteristic of As(V) coordination with no evidence of As(III) observed. Best fits of the micro-extended x-ray absorption fine structure (μEXAFS) spectra are listed in Table 3 and shown in Fig. 3. The first neighbor shell around the arsenic in +As/–P cells consisted of four oxygen ligands (Table 3) but had a second shell that is inconsistent with our As-Fe and As-S models, free AsO_4^{3-} ions, or published spectra for organo-arsenicals (Fig. 3A) (15, 16). Although other arsenical compounds such as dimethylarsinate (DMA) also have As-O and As-C bonds, they have edge positions that are shifted to lower energy from the observed As(V) and have much shorter observed As-C bond distances (16). In contrast to the models, these As-O and As-C distances are consistent with that reported from the solved crystal structure of DNA for the analogous structural position of P relative to O and C atoms (Fig. 3A) (16, 17). Therefore, our x-ray data support the position of AsO_4^{3-} in a similar configuration to PO_4^{3-} in a DNA backbone or potentially other biomolecules as well. These data are also consistent with the presence of AsO_4^{3-} in small-molecular-weight metabolites (for example, arsenylated analogs of NADH, ATP, glucose, and acetyl-CoA) as well as arsenylated proteins in which AsO_4^{3-} would substitute for PO_4^{3-} at serine, tyrosine, and threonine residues (table S3) (1, 11). Micro–x-ray fluorescence data (μXRF) further confirmed our ICP-MS measurements and showed low background P, which contrasted with regions of high arsenic correlated with high iron and zinc (Fig. 3B and fig. S2) (11). These latter two elements are routinely used as proxies for the presence of cellular material (such as C, N, and O) in our experiments because these light elements could not be detected with x-ray fluorescence under our nonvacuum conditions. However, to further support the distribution of arsenic with cellular material we used NanoSIMS to map cellular ion ratios of $^{75}As^-$:$^{12}C^-$ and $^{31}P^-$:$^{12}C^-$ (Fig. 2, B to G, and fig. S2) (11). These analyses confirmed, at a much finer resolution, that for the +As/–P condition the cells contain As with a low background of P (Fig. 2, B, D, and F). This is in contrast to the low As and higher P in –As/+P–grown cells (Fig. 2, C, E, and G). Because the x-ray absorption data

Table 2. Intracellular radiolabeled $^{73}AsO_4^-$ arsenate distribution. All major cellular subfractions contained radiolabel after cell-washing procedures. Small molecular weight (s.m.w.) metabolites potentially include arsenylated analogs of ATP, NADH, acetyl-CoA, and others (11). SE is shown.

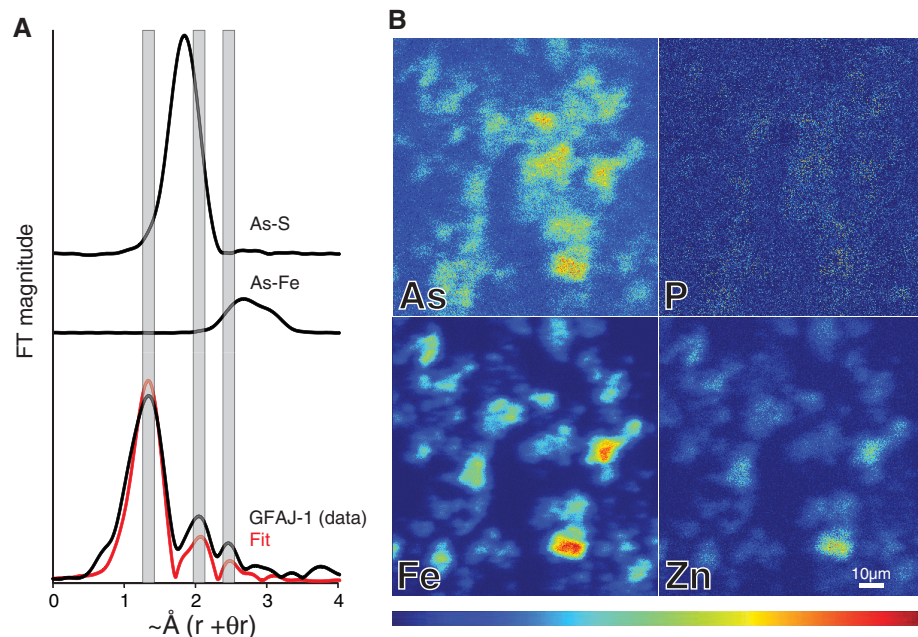| Solvent (subcellular fraction)	Cellular radiolabel recovered (percent of total)
Phenol (protein + s.m.w. metabolites)	80.3 ± 1.7
Phenol:Chloroform (proteins + lipids)	5.1 ± 4.1
Chloroform (lipids)	1.5 ± 0.8
Final aqueous fraction (DNA/RNA)	11.0 ± 0.1

Fig. 3. X-ray analysis of GFAJ-1 +As/–P described similarity of As coordinated like P in DNA. (**A**) EXAFS comparisons of the Fourier transformed data for As in model environments and GFAJ-1 (washed and fixed, collected on whole cells). Identification of each spectrum is indicated on the figure and from top to bottom are As-S, As-Fe, and GFAJ-1 data (collected on whole cells) and fit to the GFAJ-1 data (red line). (**B**) XRF maps indicated the correlation between As, iron (Fe) and zinc (Zn) and not with P with some variability but consistent with the trend that these elements are often found together (fig. S3, element correlation plots). The scale bar in the Zn quadrant of the maps is as designated and applies to all parts of the figure. Given the spatial resolution of these images, the structures identified as containing high As, Fe, and Zn are aggregates of cells. Ranges as indicated in the color bar run from cold to hot, in units of μg cm⁻², as follows: As, 0 to 1.6; P, 0 to 40; Fe, 0 to 32.1; and Zn, 0 to 2.8. Standards were used to calibrate signal and background (11).

Table 3. Results of fitting arsenic K-edge EXAFS of GFAJ-1. S02 = 1, global amplitude factor and E0 = 13.97, offset for calibration. Type, the coordination type; Number, the coordination number; R, interatomic distance; and σ^2, the measure of the static disorder of the shell. See table S2 for comparison to P in P-containing biomolecules (11).

Type	Number	R	σ^2
As-O	4.2 (0.6)	1.73 (2)	0.003 (2)
As-C	2.5 (0.5)	2.35 (4)	0.003 (2)
As-C	2.2 (0.5)	2.92 (6)	0.003 (2)

provided information about the average coordination of arsenic, our data identified a mixture of compounds in the cells. These results indicated that these compounds are dominated by arsenic(V)-oxygen-carbon–coordinated structures, and thus the bonding environment we described is consistent with our NanoSIMS data (Fig. 2A) and can be attributed to DNA. These data show that As is in the +5 redox state and bound to O and distal C atoms within acceptable covalent bond lengths, identifying AsO_4^{3-} assimilated into biomolecules within the cells in specifically relevant coordination.

Our data show arsenic-dependent growth by GFAJ-1 (Fig. 1). Growth was accompanied by AsO_4^{3-} uptake and assimilation into biomolecules including nucleic acids, proteins, and metabolites (Figs. 2 and 3 and Tables 1 and 2). In some organisms, arsenic induces specific resistance genes to cope with its toxicity (7), whereas some dissimilatory arsenic-utilizing microbes can conserve energy for growth from the oxidation of reduced arsenic species, or "breathe" AsO_4^{3-}, as a terminal electron acceptor (18). Our study differs because we used As as a selective agent and excluded P, a major requirement in all hitherto known organisms. However, GFAJ-1 is not an obligate arsenophile and grew considerably better when provided with P (Fig. 1, A and B). Although AsO_4^{3-} esters are predicted to be orders of magnitude less stable than PO_4^{3-} esters, at least for simple molecules (8), GFAJ-1 can cope with this instability. The vacuole-like regions observed in GFAJ-1 cells when growing under +As/–P conditions are potentially poly-β-hydroxybutyrate rich [as shown in other *Halomonas* species (19)], which may

stabilize As(V)-O-C type structures because nonaqueous environments appear to promote slower hydrolysis rates for related compounds (8). We propose that intracellular regions or mechanisms that exclude water may also promote this stability.

We report the discovery of an unusual microbe, strain GFAJ-1, that exceptionally can vary the elemental composition of its basic biomolecules by substituting As for P. How As insinuates itself into the structure of biomolecules is unclear, and the mechanisms by which such molecules operate are unknown.

References and Notes

1. J. Berg, J. Tymoczko, L. Stryer, *Biochemistry* (W. H. Freeman & Co., New York, ed. 6, 2007).
2. R. Hille, *Trends Biochem. Sci.* **27**, 360 (2002).
3. T. W. Lane, F. M. Morel, *Proc. Natl. Acad. Sci. U.S.A.* **97**, 4627 (2000).
4. G. Jameson, J. Ibers, in *Biological Inorganic Chemistry: Structure and Reactivity*, I. Bertini, H. Gray, I. Stiefel, J. Valentine, Eds. (University Science Books, Sausalito, CA, 2007), pp. 354–386.
5. D. Lide, Ed., *CRC Handbook of Chemistry and Physics, 90th Edition (Internet Version 2010)* (CRC Press/Taylor & Francis, Boca Raton, FL, 2010).
6. F. Wolfe-Simon, P. C. W. Davies, A. D. Anbar, *Int. J. Astrobiol.* **8**, 69 (2009).
7. B. P. Rosen, *FEBS Lett.* **529**, 86 (2002).
8. C. D. Baer, J. O. Edwards, P. H. Rieger, *Inorg. Chem.* **20**, 905 (1981).
9. R. S. Oremland, J. F. Stolz, J. T. Hollibaugh, *FEMS Microbiol. Ecol.* **48**, 15 (2004).
10. J. Switzer Blum, A. Burns Bindi, J. Buzzelli, J. F. Stolz, R. S. Oremland, *Arch. Microbiol.* **171**, 19 (1998).
11. Materials and methods are available as supporting material on *Science* Online.
12. M. Takeuchi et al., *J. Biotechnol.* **127**, 434 (2007).
13. W. Makino, J. Cotner, R. Sterner, J. Elser, *Funct. Ecol.* **17**, 121 (2003).
14. J. Mandelstam, *Bacteriol. Rev.* **24**, 289 (1960).
15. P. G. Smith et al., *Environ. Sci. Technol.* **39**, 248 (2005).
16. I. J. Pickering et al., *Plant Physiol.* **122**, 1171 (2000).
17. S. Holbrook, R. Dickerson, S. H. Kim, *Acta Crystallogr. B* **41**, 255 (1985).
18. R. S. Oremland, J. F. Stolz, *Science* **300**, 939 (2003).
19. J. Quillaguaman, O. Delgado, B. Mattiasson, R. Hatti-Kaul, *Enzyme Microb. Technol.* **38**, 148 (2006).

Correction: 3 June 2011

Supporting Online Material for

A Bacterium That Can Grow by Using Arsenic Instead of Phosphorus

Felisa Wolfe-Simon,[1,2]* Jodi Switzer Blum,[2] Thomas R. Kulp,[2] Gwyneth W. Gordon,[3] Shelley E. Hoeft,[2] Jennifer Pett-Ridge,[4] John F. Stolz,[5] Samuel M. Webb,[6] Peter K. Weber,[4] Paul C. W. Davies,[1,7] Ariel D. Anbar,[1,3,8] Ronald S. Oremland[2]

*To whom correspondence should be addressed. E-mail: felisawolfesimon@gmail.com

This PDF file includes:

Materials and Methods

Figs. S1 to S3

Tables S1 to S3

References

Correction: Several corrections and clarifications have been made to the text and tables in this file since publication. See the following pages for the specific changes made.

Page 1, paragraph 1, lines 3-5

Original:

following constitution: 0.80 mM (NH4)2SO4, 0.20 mM MgSO4·7H2O, 1.0 M NaCl, 100 mM Na2CO3, 50 mM NaHCO3, 10 mM glucose, a full complement of vitamins (*S2*) and trace elements according to Widdel et al. (*S3*) with the addition of 45 nM Na2WO4·2H2O.

Revised to:

following constitution: AML60 mineral salts (composed of 0.80 mM $(NH_4)_2SO_4$, 0.20 mM $MgSO_4 \cdot 7H_2O$, 1.0 M NaCl, 100 mM Na_2CO_3, 50 mM $NaHCO_3$ and trace elements according to Widdel et al. (*S3*) with the addition of 45 nM $Na_2WO_4 \cdot 2H_2O$) as well as 10 mM glucose and a full complement of vitamins (*S2*).

Page 1, paragraph 1, last line

Original:

All of the isolates are maintained as stock cultures in the laboratory with $AsO4^{3-}$ but no added no $PO4^{3-}$.

Revised to:
All of the isolates were maintained as stock cultures in the laboratory with AsO_4^{3-} but no added PO_4^{3-}.

Page 1, paragraph 2, line 3 (and at several other points throughout the text)

Original:

16*S* rRNA

Revised to:

16*S* ribosomal RNA sequence

Page 1, paragraph 2, line 9

Original:

Strain GFAJ-1 is maintained

Revised to:

Strain GFAJ-1 was maintained

Page 1, paragraph 3, line 4

Original:

added AsO4^{3-} and Control, no added AsO4^{3-} nor PO4^{3-}.

Revised to:

added AsO$_4^{3-}$; Control, 10 mM glucose and the required vitamins but no added AsO$_4^{3-}$ nor PO$_4^{3-}$.

Page 2, paragraph 2, line 6

Original:

Length and width were measured and volume

Revised to:

Length and width were measured for each candidate cell and volume

Page 2, paragraph 3, line 6 (and other places in the text)

Original:

or

Revised to:

nor

Page 3, paragraph 1, lines 2-3

Original:

the DNA/RNA pellet was resuspended

Revised to:

the DNA/RNA pellet was washed with 70 % ethanol, dried and then resuspended

Page 3, paragraph 2, line 8

Original:

(ten clones for each PCR product).

Revised:

(ten clones for each PCR product, one PCR product per growth condition)

Page 4, paragraph 2, line 1

Original:

Media samples were diluted and analyzed as received. The DNA/RNA gel samples,

Revised to:

AML60 mineral salts and complete medium samples were diluted and analyzed as received. AML60 mineral salts contained no added vitamins, glucose, phosphate, nor arsenate (see above in *Field site description and enrichments*). Complete medium contained all the required components and either arsenate or phosphate depending on the final additions made (denoted as +As/-P or -As/+P, respectively). The DNA/RNA gel samples,

Page 4, paragraph 2, line 5

Original:

Samples from the +As/-P, -As/+P and -As/-P conditions were prepared on separate hot plates with digestion process blanks on each hot plate to monitor for contamination (see "digestion process blank in Table S1"). The digestion process was repeated several times until solutions were clear with no precipitate.

Revised to:

Samples of AML60 mineral salts and complete media (+As/-P and -As/+P) were processed as described above on separate hot plates with digestion process blanks on each hot plate to monitor for contamination (see "digestion process blank in Table S1"). Cell wash solution, prepared as AML60 mineral salts with no added vitamins, glucose, phosphate, arsenate nor trace elements, was processed in an identical manner. The digestion process was repeated several times until solutions were clear with no precipitate.

Page 11, Table S1, line 13

Original:

MEDIA

Revised:

SOLUTIONS

Page 11, Table S1, lines 16-34, the row headings have been revised

Original:

-P/-As media (-vitamins, - arsenic, -phosphate, - glucose)
5 Apr 2010 batch
-P/-As media (-vitamins, - arsenate -phosphate, - glucose)
11 June 201 batch
-P/+As media (+vitamins, +10 mM glucose, + arsenate)
29 July 2010 batch
-P/+As media (+ vitamins, +10 mM glucose, +arsenate)
5 Apr 2010 batch
+P/-As media (+ vitamins, +10 mM glucose, + phosphate)
5 Apr 2010 batch
cell wash solution -P/-As media
(-vitamins, - arsenic, -phosphate, - glucose, - trace metals),
3 July 2010 batch

Revised to:

AML60 mineral salts (-As/-P)
(-vitamins, -glucose, -arsenate, -phosphate)
5 Apr 2010 batch
 AML60 mineral salts (-As/-P)
(-vitamins, -glucose, -arsenate, -phosphate)
11 June 2010 batch
+As/-P complete medium
(+vitamins, +glucose, +arsenate)
29 July 2010 batch
+As/-P complete medium
(+vitamins, +glucose, +arsenate)
5 Apr 2010 batch
-As/+P complete medium
(+vitamins, +glucose, +phosphate)
5 Apr 2010 batch
cell wash solution, AML60 mineral salts, no TE
(-As/-P)
(-vitamins, -glucose, -arsenate, -phosphate, -trace
elements)
 3 July 2010 batch

Table S2, line 8

Original:

GJAJ

Revised:

GFAJ-1

Supporting online material for:
"A bacterium that can grow by using arsenic instead of phosphorus"

MATERIALS AND METHODS

Field site description and enrichments. Mono Lake bottom sediment was added to 20-ml sterile glass screw top tubes containing 10 ml autoclaved artificial defined Mono Lake medium (AML60; *S1*) at pH 9.8 with the following constitution: AML60 mineral salts (composed of 0.80 mM $(NH_4)_2SO_4$, 0.20 mM $MgSO_4 \cdot 7H_2O$, 1.0 M NaCl, 100 mM Na_2CO_3, 50 mM $NaHCO_3$ and trace elements according to Widdel et al. (*S3*) with the addition of 45 nM $Na_2WO_4 \cdot 2H_2O$) as well as 10 mM glucose and a full complement of vitamins (*S2*). All materials were prepared with sterile- and nutrient-clean techniques. Cultures were grown in tubes at room temperature (20 to 22°C) in the dark. Control tubes were set up with added phosphate (P: 0.6 mM KH_2PO_4 + 0.9 mM K_2HPO_4) while experimental tubes had no added PO_4^{3-}, and a gradient of added $Na_2HAsO_4 \cdot 7H_2O$: 100μM, 1mM and 5mM. Seven successive decimal dilution transfers, over the course of three months with an overall dilution of 10^{-7} from the original inocula, resulted in modest increased turbidity in all tubes, as compared with a sterile control. The sixth transfer of the 5mM AsO_4^{3-} (no added PO_4^{3-}) condition was closely monitored and demonstrated an approximate growth rate (μ) of 0.1 day^{-1}. 5 mM AsO_4^{3-} cultures were then spread on plates containing AML60 1.5 % solid agar (10 mM glucose, 5 mM AsO_4^{3-}, no PO_4^{3-}). Two types of colony morphologies were observed. Single colonies were picked and reintroduced into defined artificial liquid AML60 with 10 mM glucose, 5 mM AsO_4^{3-}, and no PO_4^{3-}. All of the isolates were maintained as stock cultures in the laboratory with AsO_4^{3-} but no added PO_4^{3-}.

Isolation of strain GFAJ-1. Of the colonies picked and cultured back into liquid medium, a single colony, GFAJ-1, was identified as the fastest growing isolate and pursued for further study. After identification of GFAJ-1 by 16*S* ribosomal RNA sequence phylogeny (see below) as a member of the Halomonadaceae and closely related to microbes known to survive high arsenate concentrations, we tested the growth of GFAJ-1 over the range of 10, 20, 40 and 80 mM AsO_4^{3-}. We determined the +As/-P condition that elicited the best growth for GFAJ-1 was AML60 amended with 10 mM glucose, 40 mM AsO_4^{3-}, no PO_4^{3-} and incubated at 28°C. All experimental evidence shown for this study were conducted with GFAJ-1 cells grown under these conditions identified in the main manuscript text as "+As/-P" unless explicitly stated otherwise. Strain GFAJ-1 was maintained as a stock culture for all inocula under the +As/-P condition.

GFAJ-1 growth experiment. GFAJ-1 cells were grown in 10 ml total volume in 20-ml screw-top glass tubes in sterile AML60 amended 10 mM glucose and vitamins (as above) under three experimental conditions including +As/-P, 40 mM AsO_4^{3-} with no added PO_4^{3}; -As/+P, 1.5 mM PO_4^{3-} with no added AsO_4^{3-}; Control, 10 mM glucose and the required vitamins but no added AsO_4^{3-} nor PO_4^{3-}. Six replicates of +As/-P and -As/+P with two replicates of Control experimental tubes were set up. All tubes were incubated at 28°C in the dark. We measured the optical density of all cultures at 680 nm

(OD_{680}) on a Spectronic 20 Genesys spectrophotometer (Spectronic Instruments). Because we had to remove samples for acridine orange direct cell count (AODC) measurements (*S4*), O.D. was performed on all cultures (n=6 for experimental tubes and n=2 for control tubes) until material was depleted due to sampling as of 262 hours of the experiment. AODCs were done on a subset of the cultures (n=3 for experimental and n=1 for control tubes) to allow enough material for the duration of the experiment. AODCs were done according to standard protocols outlined elsewhere (*S5*).

Electron microscopy. GFAJ-1 was grown +As/-P and -As/+P to stationary phase for EM analyses. For scanning electron microscopy, critical point drying was performed in a Ladd Critical Point Dryer No. 28000 using CO_2 as the transitional fluid. Cells were sputter coated with Au/Pd and imaged at 5 kV with a Leo 982 Digital Field Emission Electron Microscope. Cells volumes were estimated using ImageJ (rsb.info.nih.gov/ij/; *S6, S7*) with n= 6 cells measured for both +As/-P and -As/+P conditions. Length and width were measured for each candidate cell and volume was estimated based on a cylindrical shape. Transmission electron microscopy preparation included negative staining of whole cells performed with 1 % uranyl acetate on Formvar-coated grids. Thin sections of Spurr's embedded samples were prepared following the procedure described by Switzer Blum et al. 1998 (*S8*). Samples were observed with a transmission electron microscope (100CX; JEOL) at 60 kV.

Radiolabel $^{73}AsO_4^{3-}$ experiment. Cells were grown in duplicate 100 ml cultures in 250-ml screw top glass flasks in the dark at 28°C in AML60 with 10 mM glucose, 20 mM AsO_4^{3-}, without added PO_4^{3-} and amended with 111 kBq ml^{-1} of the radiolabel $^{73}AsO_4^{3-}$ (carrier-free, Oak Ridge National Laboratory, Oak Ridge, TN). To determine uptake and cellular distribution of $^{73}AsO_4^{3-}$ cells were grown to stationary phase, collected by centrifugation and washed three times with AML60 containing no PO_4^{3-}, AsO_4^{3-}, vitamins nor glucose so as to remove any adsorbed radiolabel. Cell pellets were processed for nucleic acid extraction (see below). The radiolabel was quantified by gamma spectrometry (*S9, S10*) to determine radiolabel distribution in all subcellular fractions of the extraction including the phenol subnatant, three phenol:chloroform subnatants, chloroform subnatant, final aqueous supernatant and DNA/RNA pellet. To estimate the total As associated with a genome, we downloaded the size of all sequenced bacterial genomes and calculated a conservative estimate for the total P associated with the number of base pairs in a bacterial genome on average. These data are publically available from the JGI website.

Nucleic acid extraction. To separate cellular fractions and isolate DNA and RNA, cell pellets were disrupted using a buffer containing 1.2 % SDS, 30 mM EDTA, 50 mM Tris-HCl (pH 8.0), 220 mM NaCl and 50 mM β-mercaptoethanol. Extractions were initiated with a phenol addition (pH 6.6), briefly vortexed, and separated by centrifugation. The extraction was further clarified by three phenol:chloroform (1:1, pH 6.7) additions and centrifugation, where the supernatant (aqueous) fraction was serially removed and extracted with phenol:chloroform. The third aqueous supernatant from the phenol:chloroform steps was combined with equal part chloroform and centrifuged. The DNA/RNA was precipitated from the chloroform step supernatant by addition of one-tenth volume 3 M sodium

acetate (pH 5.5) and pre-chilled 100 % ethanol. The nucleic acids were pelleted by centrifugation and the supernatant removed. For downstream molecular biology applications, the DNA/RNA pellet was washed with 70 % ethanol, dried and then resuspended in sterile molecular biology grade water.

Phylogenetic analyses. Cells were harvested that had been grown under four conditions: +As/-P, -As/+P, +As/+P and -As/-P (control). DNA extractions were done as explained above. The 16*S* ribosomal RNA gene was amplified by PCR using the universal primers Bact 8F 5'- AGA GTT TGA TCC TGG CTC AG-3' and Univ 1517R 5'- ACG GCT ACC TTG TTA CGA CTT-3' (Integrated DNA Technologies, Inc. Coralville, IA). PCR products were run out on 1% agarose gels, bands cut, and gel-purified using QIAquick Gel Extraction Kit (#28704, Qiagen, Inc. Valencia, CA). Gene fragments were then cloned into *E. coli* (pCR4 TOPO-TA kit #K4575-01, Invitrogen, Inc. Carlsbad, CA) and a total of forty clones were picked for sequencing (ten clones for each PCR product, one PCR product per growth condition). Positive clones were isolated using QIAprep Spin Miniprep Kit (#27106, Qiagen, Inc. Valencia, CA) verified by PCR for correct insert and sent for sequencing (Sequetech, Inc. Mountain View, CA). All conditions produced identical 16*S* ribosomal RNA gene sequences; hence a single sequence was used representing GFAJ-1 for tree construction (Figure S1). 16*S* ribosomal RNA sequences were aligned employing the NAST alignment tool (*S11*) as part of the Greengenes Database and Tools (*S12*). The sequences were also tested to identify any possible PCR produced chimeras using the Bellerophon package (*S13*) and preliminary taxa identification was done using the Ribosomal Database Project tools and pipeline (*S14*). After the final alignment was manually adjusted using BioEdit (*S15*) the tree was constructed using a maximum likelihood analysis with PhyML (*S16*) through the PhyML software package accessed through the Phylemon online tools suite (phylemon.bioinfo.cipf.es). Sequences used for analysis are listed in Table S3. The sequence for GFAJ-1 has been deposited with GenBank (accession HQ449183).

Total elemental composition of GFAJ-1, medium and buffers by ICP-MS. Phospho-molybdenum blue has lower detection limits for phosphate concentrations, but was not used due to the arsenate interference (*S17*). Batch cultures were grown until early stationary phase and harvested by centrifugation. Cell pellets were gently washed three times by resuspension in AML60 containing no added PO_4^{3-}, AsO_4^{3-}, vitamins, glucose nor trace elements to wash any potentially adsorbed inorganic minerals from the cell surfaces. Cells were then flash frozen until acid digestion. Cell pellets were digested in concentrated nitric acid until completely dissolved, dried and then re-dissolved in 0.32 M nitric acid. Other washed cell pellets were processed as for nucleic acid extraction (see above section) and the "phenol" and "final aqueous and pellet" fractions were dried, dissolved and acidified in a similar manner to the whole cell pellets (presence of the DNA in the samples was confirmed by measuring the absorption properties of the sample at 260 nm prior to processing). DNA/RNA fractions were also run out on 1 % agarose gels, positive and control (not containing DNA or RNA) bands excised and subject to the same ICP-MS preparation (dried, dissolved and acidified) as the cell pellets. Details below.

All reagent acids were trace metal grade; pipette tips and centrifuge tubes were precleaned by soaking in dilute Citranox overnight, washed three times in 18.2 MΩ water, soaked in 20% (v/v) reagent grade nitric acid for several days, washed three times in 18.2 MΩ water, soaked in 20% (v/v) reagent grade hydrochloric acid for several days, washed three times in 18.2 MΩ water and dried in a designated HEPA-filtered hood. Savillex Teflon digestion vessels were cleaned by soaking in dilute Micro90 detergent, rinsed three times in 18.2 MΩ water, heated to sub-boiling in 50% (v/v) reagent grade nitric acid for 24 hours, rinsed three times in 18.2 MΩ water, heated to sub-boiling in 50% (v/v) reagent grade hydrochloric acid for 24 hours, rinsed three times in 18.2 MΩ water, heated to sub-boiling in 18.2 MΩ water for 18 hours, dried in a designated HEPA-filtered hood. An additional cleaning step of 50% (v/v) trace metal grade nitric acid heating for each container on a hot plate was completed to reduce any potential contamination or blank contribution.

AML60 mineral salts and complete medium samples were diluted and analyzed as received. AML60 mineral salts contained no added vitamins, glucose, phosphate, nor arsenate (see above in *Field site description and enrichments*). Complete medium contained all the required components and either arsenate or phosphate depending on the final additions made (denoted as +As/-P or -As/+P, respectively). The DNA/RNA gel samples, the DNA/RNA extracts, the phenol extracts and the washed cell pellets were digested in a class 10 hood in a trace metal clean lab. The samples were weighed, transferred into Savillex Teflon digestion vials, dried under filtered air at low temperature and weighed again. 2 ml of trace metal clean nitric acid was added to each sample, and they were digested in a closed vessel overnight at ~150°C. Samples of AML60 mineral salts and complete media (+As/-P and -As/+P) were processed as described above on separate hot plates with digestion process blanks on each hot plate to monitor for contamination (see "digestion process blank in Table S1"). Cell wash solution, prepared as AML60 mineral salts with no added vitamins, glucose, phosphate, arsenate nor trace elements, was processed in an identical manner. The digestion process was repeated several times until solutions were clear with no precipitate. The phenol samples were digested in aqua regia until they were clear with no precipitate.

Samples were analyzed on a Thermo X-series quadrupole ICP-MS with Collision Cell Technology (CCT) option at the W.M. Keck Foundation Laboratory for Environmental Biogeochemistry at Arizona State University in Tempe, AZ. Low P and As sample concentrations, combined with the high ionic strength of media (Na/P ratio up to 10^6) and samples can cause plasma suppression. Hence, the following precautions were taken to assure accuracy and validity of measured concentrations: a) multiple calibration curves, b) standard addition for As and P for most samples except in cases of sample limitation, c) independent single element check standards at concentrations similar to samples, d) independent sample matrix-matched check standards e) frequent analytical blanks f) multiple process blanks g) replicate digestions from the same sample and h) repeat analyses of samples over multiple analytical sessions. The calibration curve used a multi-element standard solution, and was analyzed at the beginning, end and approximately every fifty samples during the runs. Sc, Ge, Y, In and Bi were used as internal standards. As was analyzed using a 7% H_2 in He gas mixture to reduce

polyatomic interferences. Blanks and secondary single element standards of similar concentration of As and P as the samples were analyzed as check standards every five samples. Matrix matched secondary standards were designed to evaluate accuracy of low P and As concentration determinations in the high salt matrix of many samples and included A) 100 ppm Na, B) 700 ppb Na 10 ppb P 1 ppb As, C) 50 ppm Na 3 ppm P 10 ppb As, D) 50 ppm Na 5 ppb P, and E) 50 ppm Na 5 ppb P 140 ppb As; these samples showed good reproducibility within error. From the reproducibility of single element and matrix-matched check standards, limit of detection is approximately 1 ppb for both As and P.

Digested samples were diluted by gravimetry to a dilution factor of 30 and analyzed by ICP-MS to obtain a rough estimate of As and P concentrations. Subsequently, each sample was measured by standard addition of As and P in amounts appropriate to that sample. Depending on sample availability, each sample was measured using a standard addition curve comprised of with three to five measurements per curve. The correlation coefficient of 18 of the 22 phosphorus standard addition curves was better than 0.95; the other four were 0.52, 0.71, 0.88 and 0.93. The correlation coefficient of 19 of the 22 arsenic standard addition curves was better than 0.95; the other three were 0.58, 0.82 and 0.93. The data for the three P standard addition curves and two As standard addition curves with correlation coefficients less than 0.9 are denoted in italics in Table S1. Samples not analyzed by standard addition due to limited sample quantities are in italics in Table S1. "Repeat" in Table S1 indicates a replicate digestion and analysis.

NanoSIMS analyses. Individual cells and DNA in high purity agarose gel sections were analyzed for As and P abundance by high-resolution secondary ion mass spectrometry (SIMS) on a Cameca NanoSIMS 50 at Lawrence Livermore National Laboratory (LLNL) in Livermore, California. The NanoSIMS 50 allows the simultaneous collection of 5 isotopes with high spatial resolution (up to 50 nm) and high mass resolution. Glutaraldehyde preserved washed GFAJ-1 cells were first coated with 5 nm of iridium (agarose slices were gold coated to ~20 nm) to make them conductive, then a focused Cs^+ primary beam was rastered over the sample surfaces to generate secondary ions ($^{12}C^-$, $^{12}C^{14}N^-$, ^{31}P, $^{34}S^-$, and $^{75}As^-$ for the cell analyses and $^{12}C^-$, $^{29}Si^-$, ^{31}P, $^{70}Ge^-$, and $^{75}As^-$ for agarose analyses) along with secondary electron (SE) images. Cells were sputtered with Cs^+ at high beam current before measurements to achieve sputtering equilibrium. For cell analyses, a 2.2 pA Cs^+ primary beam focused to a nominal spot size of 100-150 nm was stepped over the sample in a 128 x 128 pixel raster to generate secondary ions, collected by electron multipliers with a dead time of 44 ns. Dwell time was 1ms/pixel, and raster size was either 3 x 3 μm or 8 x 8 μm. DNA gel samples were sputtered with Cs^+ at moderately high beam current (~100 pA) to a depth of ~100 nm before performing the analyses with ~10 pA Cs^+ on a 5 x 5 μm, 128 x 128 pixel raster with 2 ms/pixel dwell time and 14 cycles. To resolve As from neighboring isobaric interferences at mass 75, the mass spectrometer was tuned to ~8000 mass resolving power and the $^{75}As^-$ peak was aligned on a GaAs wafer. Samples were simultaneously imaged by secondary electrons which yields a reference image useful for comparison to the secondary ion images. Secondary ions were detected in simultaneous collection mode by pulse counting to

generate 30-60 serial quantitative secondary ion images (*i.e.* layers). Measurements were repeated on 10 to 25 individual cells per treatment (+As/-P, -As/+P), and at 4 to 7 different locales in the DNA-loaded agarose gels. For the cell analysis, each was defined as a region of interest (ROI) by encircling pixels where $^{12}C^{14}N^-$ counts > 30% of the maximum counts in the image. The As:C and P:C composition of each ROI was calculated by averaging over all replicate layers where both $^{12}C^-$ and $^{12}C^{14}N^-$ count rates were stable (i.e., at sputtering equilibrium). Data were processed as quantitative elemental ratio images using LIMAGE software, developed by L. Nittler (Carnegie Institution of Washington, Washington, D.C.), and were corrected for detector dead-time and image shift from layer to layer (due to drift in the location of the ion beam). Concentration estimates of As and P were calculated with:

$$[X] = RSF_{X/C} * (^nX^-/^{12}C^-)$$

where [X] is the concentration of the element of interest in hydrated agarose, $RSF_{X/C}$ is the relative sensitivity factor for element X relative to carbon, and $^nX^-$ and $^{12}C^-$ are the measured isotopes. $RSF_{X/C}$ is estimated based on NanoSIMS and ICP-MS data for bulk gel samples in this study, based on wet weight ($RSF_{As/C} \sim 1.2 \times 10^{-3}$ g As · g^{-1} agarose · $(^{75}As^-/^{12}C^-)^{-1}$; $RSF_{P/C} \sim 1.2 \times 10^{-3}$ g P · g^{-1} agarose · $(^{31}P^-/^{12}C^-)^{-1}$). Because of significant uncertainty in bulk gel P and particularly As concentrations, the precisions of the RSF and subsequent concentration estimates are low relative to the precisions of the ion ratios and therefore the relative concentrations. The relative ratio of $RSF_{As/C}$ to $RSF_{P/C}$ is ~2 compared to 7 based on published values for silicon wafer (*S18*).

Synchrotron Studies. GFAJ-1 cells were collected by centrifugation and washed two times with AML60 with no added PO_4^{3-}, AsO_4^{3-}, vitamins nor glucose and fixed at a final concentration of 0.25% glutaraldehyde. Samples were air dried on Nucleopore 0.2 μm polycarbonate filters and directly subjected to beam radiation. Data were recorded at the As K-edge (11867 eV) on beam line 2-3 at the Stanford Synchrotron Radiation Lightsource (SSRL). The beam at BL2-3 is micro-focused using Kirkpatrick-Baez mirrors to a size of 2x2 microns. The sample was rastered across the x-ray beam and the elemental fluorescence at each pixel was measured in a continuous manner. Areas of interest were selected by identifying groups of cells on the sample. EXAFS data were collected at several points of interest, from 200 eV below the edge to 650 eV above the edge (k of 13). X-ray absorption spectra were averaged, background subtracted and processed using the SIXPACK software (*S19*). The extracted EXAFS data were fit using shell-by-shell fitting in SIXPACK, using algorithms from IFEFFIT (*S20*), and theoretical phase and amplitude calculations obtained from FEFF7 (*S21*).

Correlation plots (Figure S3) were created by plotting the concentrations of each element at each pixel in the map. Elemental concentrations were determined by calibration of the fluorescence intensity of each element excited with 12 keV x-rays. A total of 400 pixels were used for each elemental calibration. Metal foil standards were obtained from Micromatter (Vancouver Canada). Due to the low response of some of the elements, the pixel intensities were "smoothed" using an adjacent averaging

kernel, i.e. the intensity of a pixel was averaged with the 8 other pixels that are adjacent. This process reduces the pixelation of single photon counting.

Supplementary Figures.
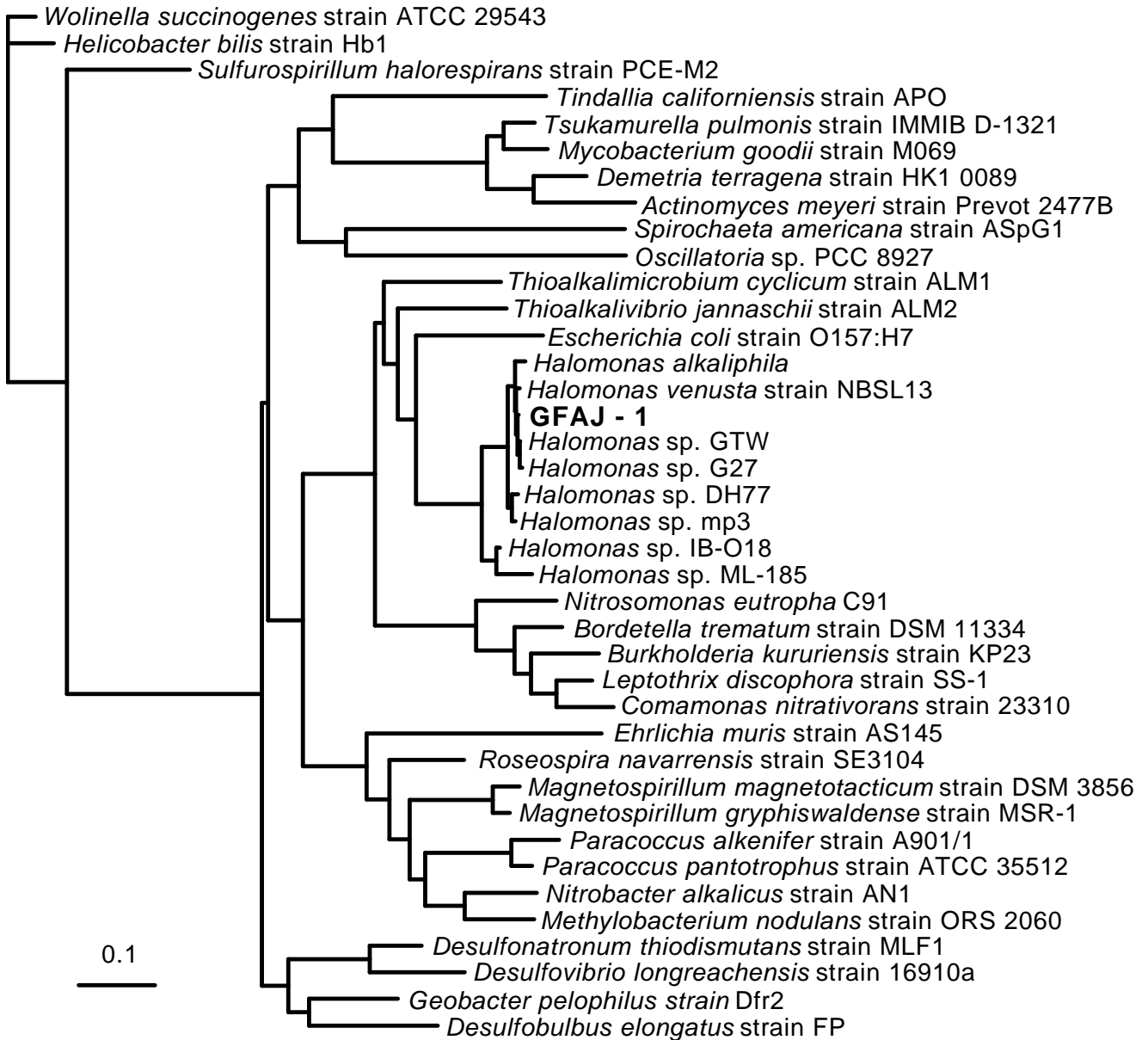
Figure S1. Phylogenetic analysis of strain GFAJ-1. Maximum likelihood phylogenetic tree based on 16*S* ribosomal RNA gene sequences identified GFAJ-1 as a member of the Halomonadaceae family in the Gammaproteobacteria.
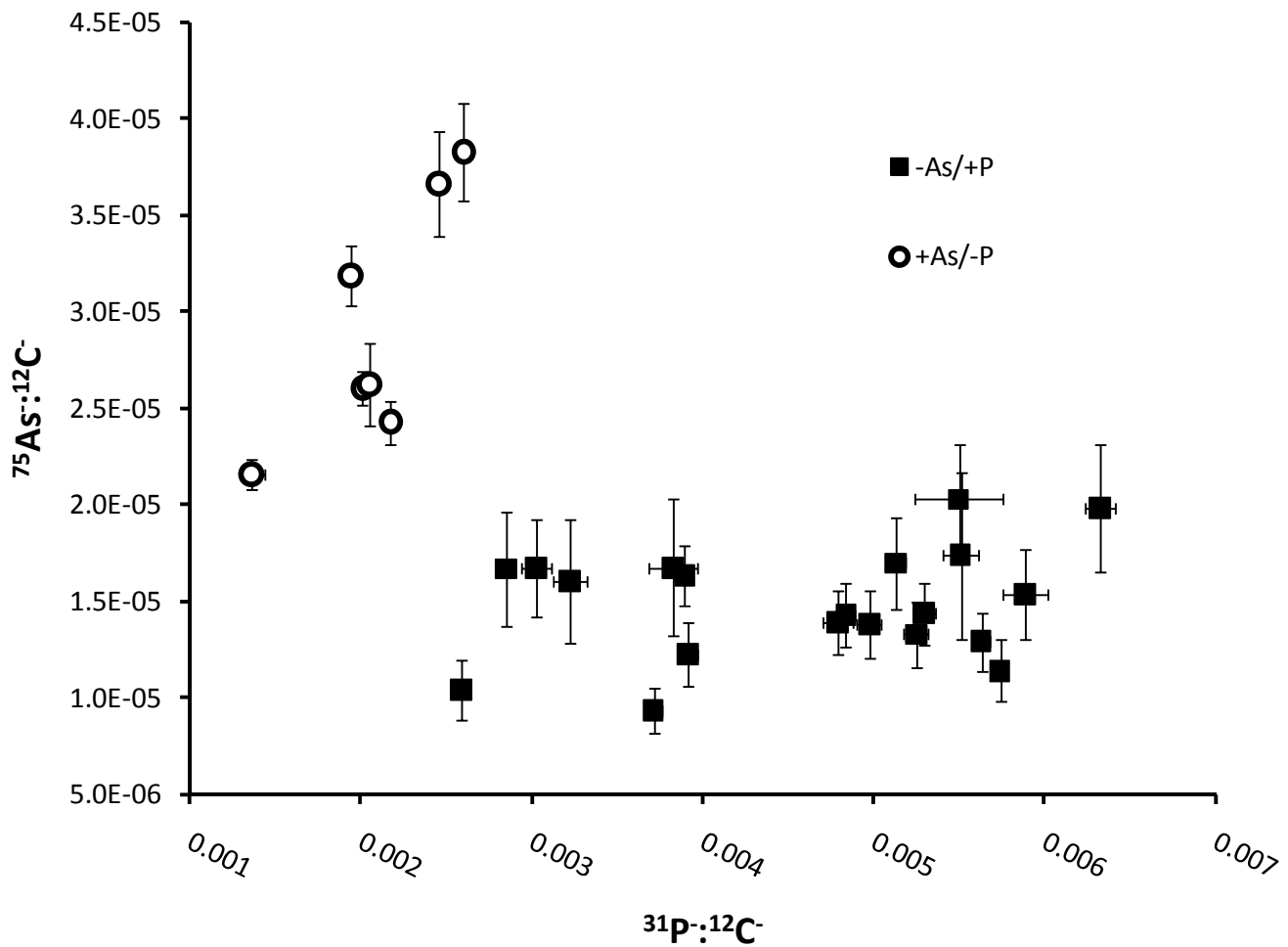
Figure S2. ^{75}As$^-$:^{12}C$^-$ versus ^{31}P$^-$:^{12}C$^-$ ratio plot from GJAJ-1 cells by NanoSIMS. Data showing the relationships between As, P and C for GFAJ-1 cells grown +As/-P (open circles) and -As/+P (closed squares). Error bars represent 1 standard deviation of analytical variance during a single measurement.
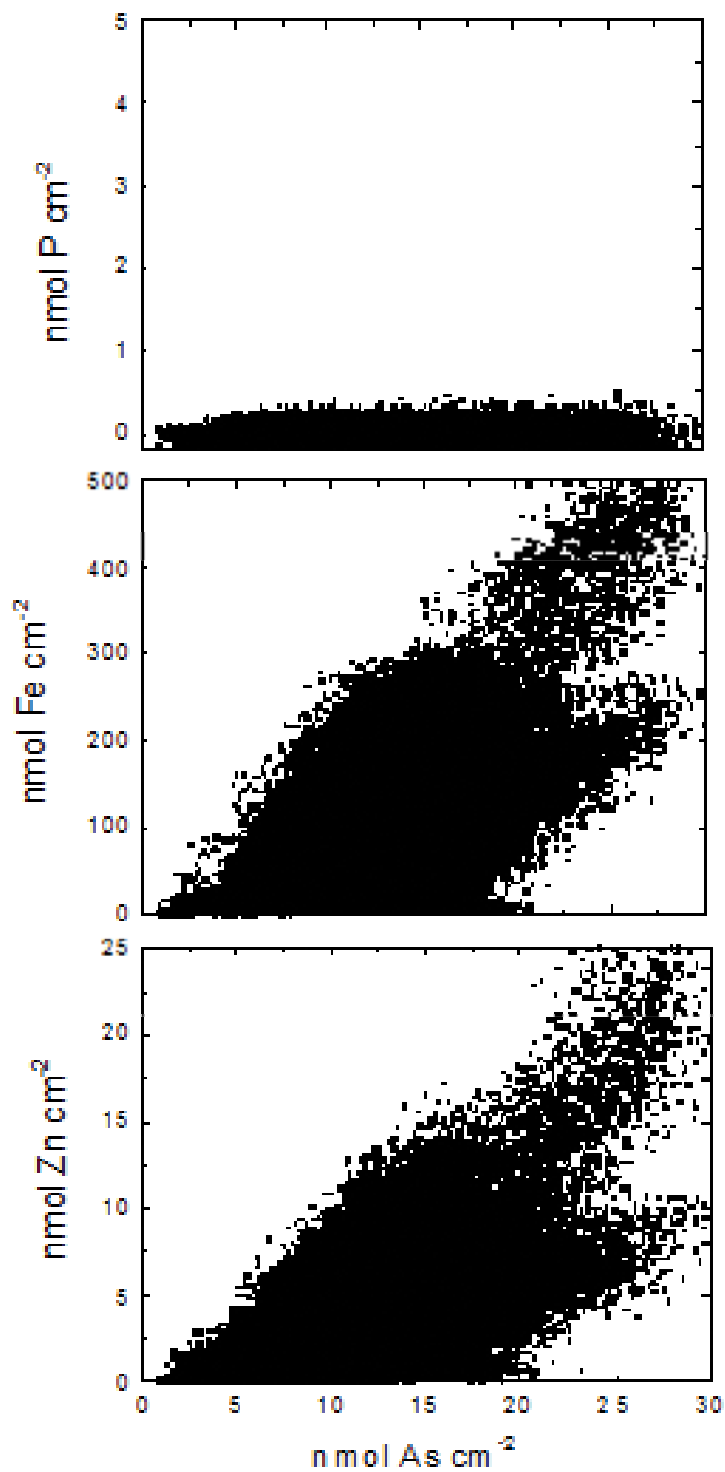
Figure S3. Correlation plots of P, Fe, and Zn versus As XRF mapping data for GFAJ-1 cells.
Correlation plots showing the relationship of the spatial distribution of phosphorus (top), iron (middle) and zinc (bottom) with respect to arsenic for the images and data shown in Figure 3B. Strong correlations exist between Fe, Zn and As while there is no correlation between As and P.

Supplementary Tables

Table S1. ICP-MS analyses.[*]

|	P ng	+/-[c]	As ng	+/-[c]	As/P	+/-[d]
BLANKS						
sterile falcon tube blank	*<1*		*<1*			
repeat	*<1*		*<1*			
+As/-P digestion process blank	*<1*		*<1*			
repeat	*<1*		*<1*			
-As/+P digestion process blank	*<1*		*<1*			
repeat	*<1*		*<1*			
+As/+P digestion process blank	*<3*		*<1*			
gel blank	795[a]	80	42.5[a]	9		
repeat	1,066	107	<2			
repeat	599	60	<2			
SOLUTIONS	**μM**		**μM**			
water blank	*<0.03*		*<0.01*			
repeat	*<0.03*		*<0.01*			
AML60 mineral salts (-As/-P) (-vitamins, -glucose, -arsenate, -phosphate) 5 Apr 2010 batch	3.7	0.4	0.26	0.03		
AML60 mineral salts (-As/-P) (-vitamins, -glucose, -arsenate, -phosphate) 11 June 2010 batch	<0.3		0.43	0.04		
+As/-P complete medium (+vitamins, +glucose, +arsenate) 29 July 2010 batch	2.9	0.3	33,520	3,352		
+As/-P complete medium (+vitamins, +glucose, +arsenate) 5 Apr 2010 batch	2.7	0.3	39,920	3,992		
-As/+P complete medium (+vitamins, +glucose, +phosphate) 5 Apr 2010 batch	2,003	200	0.16	0.02		
cell wash solution, AML60 mineral salts, no TE (-As/-P) (-vitamins, -glucose, -arsenate, -phosphate, -trace elements) 3 July 2010 batch	*7.4[a]*	23	*<0.01[a]*			

Table S1continued. ICP-MS analyses.[*]

DNA/RNA EXTRACTS, GELS AND PHENOL SAMPLES	P ppb	+/-[c]	As ppb	+/-[c]	As/P	+/-[d]
+As/-P DNA/RNA extract GFAJ	*2,081*	*174*	*<20*			
-As/+P DNA/RNA extract	266,000[a]	26,600	118	35.3		
+As/-P DNA/RNA GFAJ gel	*2,339*	*117*	*89*	*18*	*0.038*	*0.008*
+As/-P RNA gel	455	46	<1		-	
-As/+P DNA/RNA GFAJ gel	1,820	180	12	2	0.007	0.0015
-As/+P RNA gel	4,063	406	6.3	1.3	0.002	0.0003
-As/+P gel	6,110	610	<1		-	
-As/+P phenol	241,100	12,100	3,650	365	0.02	0.0017
repeat	269,100	29,100	3,717	370	0.01	0.002
+As/-P phenol	4,170	830	4,880	770	1.17	0.30
repeat	4,670	930	4,570	460	0.98	0.22

CELLS	dry wt %		dry wt %			
+As/-P cells[b]	*0.023*	*0.002*	*0.114*	*0.011*	*4.91*	*0.69*
repeat[b]	*0.023*	*0.002*	*0.200*	*0.020*	*8.55*	*1.21*
repeat[b]	*0.024*	*0.002*	*0.624*	*0.062*	*26.56*	*3.76*
repeat[b]	*0.036*	*0.004*	*0.550*	*0.055*	*15.19*	*2.15*
+As/-P cells	0.014	0.001	0.010	0.001	0.76	0.08
repeat	0.011	0.001	0.010	0.001	0.97	0.11
repeat	0.011	0.001	0.009	0.001	0.83	0.09
repeat	0.011	0.001	0.011	0.001	0.95	0.11
average	0.019	0.009	0.191	0.25	**7.3**	**9.3**
-As/+P cells[b]	*0.66*	*0.07*	*0.0006*	*0.0001*	*0.0004*	*0.0001*
repeat[b]	*0.23*	*0.02*	*0.0005*	*0.00005*	*0.0011*	*0.0002*
-As/+P cells	0.63	0.06	0.0015	0.0001	0.0023	0.0003
repeat	0.65	0.06	0.0015	0.0001	0.0022	0.0003
average	0.542	0.210	0.0010	0.00053	**0.0015**	**0.0009**

[*] [a]Correlation coefficient of sample addition curve was between 0.58 and 0.9. [b]Sample was from batch grown in June 2010. All other samples were grown in a separate batch in July 2010. [c]Errors are calculated as the standard deviation on replicate analyses or 10%, whichever is larger. [d]Error is the expanded error including uncertainties on measurements. "Repeat" indicates a replicate sample digestion and analysis. Sample names in italics designates that the sample was analyzed in several dilutions and on multiple analytical sessions with separate calibration curves, but not as standard addition curves.

Table S2. NanoSIMS gel elemental concentrations and ion ratios.[†]

	P ppb[a]	+/-[b]	As ppb[c]	+/-	As/P g/g	As/P atom/atom	$^{31}P^-/^{12}C^-$	+/-	$^{75}As^-/^{12}C^-$	+/-	$^{75}As^-/^{31}P^-$
+As/-P DNA	299	36	27	5	0.09045	0.03738	2.52E-04	3.06E-05	1.34E-05	2.48E-06	5.31E-02
-As/+P DNA	1017	237	14	3	0.01361	0.00562	8.58E-04	2.00E-04	6.85E-06	1.56E-06	7.99E-03
-As/+P RNA	1202	93	5	1	0.00411	0.00170	1.01E-03	7.81E-05	2.45E-06	5.25E-07	2.41E-03
Blank[d]	820	143	15	3	0.01829	0.00756	6.92E-04	1.21E-04	7.43E-06	1.50E-06	1.07E-02

[†]Measurements are mean values for splits of excised agarose gel bands loaded with purified GFAJ-1DNA and RNA; the other portion was run by ICP-MS. [a, c]Elemental concentrations are for hydrated agarose. [b]All error values reported in this table are 2 * standard error. [d]Blank values were measured on agarose gel segments excised from outside of electrophoresis lanes; these are an upper limit of expected background ion concentrations caused by trace impurities in agarose, loading dye or ethidium bromide stain.

Table S3. Various bond length distances of typical phosphate containing biomolecules between phosphorus, oxygen and carbon atoms.[‡]

Compound (PDB ID)	Type P-O	P-C	P-P	P-C$_2$
ATP (ANP)	1.69 1.75 1.76	2.91	3.24	-
NAD (NAD)	1.65 1.78	2.70	2.86	4.24
Glucose-6-phosphate (B6G)	1.49 1.62	2.45	-	3.86
acetyl-CoA (ACO)	1.50 1.64	2.49	2.63	3.65 3.91
Glycogen synthase kinase-3β inhibitor complex (3F88)	1.46 1.55 1.56 1.58	2.51	-	3.35 3.38
DNA (7BNA)	1.47 1.58	2.52 2.66	-	3.36 3.76 3.97 4.14

[‡]These structures were taken directly from the protein databank (www.pdb.org, *S22*) and are "ligand structures" standards in the PDB while 3F88 is an example of a phosphorylated protein. They have been identified in a range of biomolecules.

Table S4: Sequences used for phylogenetic tree construction

Taxon	Accession
Actinomyces meyeri strain Prevot 2477B	NR_029286
Bacillus selenitireducens strain MLS10	NR_028707
Bordetella trematum strain DSM 11334	NR_025404
Burkholderia kururiensis strain KP23	NR_024721
Comamonas nitrativorans strain 23310	NR_025376
Demetria terragena strain HK1 0089	NR_026425
Desulfobulbus elongatus strain FP	NR_029305
Desulfonatronum thiodismutans strain MLF1	NR_025163
Desulfovibrio longreachensis strain 16910a	NR_029364
Ehrlichia muris strain AS145	NR_025962
Escherichia coli strain O157:H7	EU118103
Geobacter pelophilus strain Dfr2	NR_026077
Halomonas alkaliphila	AJ640133
Halomonas sp. DH77	FJ404755
Halomonas sp. G27	EF554887
Halomonas sp. GTW	DQ279849
Halomonas sp. IB-O18	AM490136
Halomonas sp. ML-185	AF140007
Halomonas sp. mp3	AJ551117
Halomonas venusta strain NBSL13	FJ973521
Helicobacterbilis strain Hb1	NR_029182
Leptothrix discophora strain SS-1	NR_025916
Magnetospirillum gryphiswaldense strain MSR-1	NR_027605
Magnetospirillum magnetotacticum strain DSM 3856	NR_026381
Methylobacterium nodulans strain ORS 2060	NR_027539
Mycobacterium goodii strain M069	NR_029341
Nitrobacter alkalicus strain AN1	NR_024920
Nitrosomonas eutropha C91	NR_027566
Oscillatoria sp. PCC 8927	GQ351575
Paracoccus alkenifer strain A901/1	NR_026424
Paracoccus pantotrophus strain ATCC 35512	NR_026457
Roseospira navarrensis strain SE3104	NR_025440
Spirochaeta americana strain ASpG1	NR_028820
Sulfurospirillum halorespirans strain PCE-M2	NR_028771
Thioalkalimicrobium cyclicum strain ALM1	NR_028806
Thioalkalivibrio jannaschii strain ALM2	NR_028807
Tindallia californiensis strain APO	NR_025162
Tsukamurella pulmonis strain IMMIB D-1321	NR_029302
Wolinella succinogenes strain ATCC 29543	NR_025942

Supplementary References

S1.   J. Switzer Blum, A. B. Bindi, J. Buzzelli, J. F. Stolz, R. S. Oremland, *Arch Microbiol* **171**, 19 (1998).

S2.   R.S. Oremland, J. Switzer Blum, C.W. Culbertson, P.T. Visscher, L.G. Miller, P. Dowdle and F.E. Strohmaier, *Appl Environ Microbiol* **60**, 3011 (1994).

S3.   F. Widdel, G. Kohring, F. Mayer, *Arch Microbiol* **134**, 286 (1983).

S4.   J. Hobbie, R. Daley, S. Jasper, *Appl Environ Microbiol* **33**, 1225 (1977).

S5.   R. Oremland *et al.*, *Science* **308**, 1305 (2005).

S6.   M. D. Abramoff, Magelhaes, P.J., Ram, S.J., *Biophotonics Int* **11**, 36 (2004).

S7.   W. S. Rasband. (U. S. National Institutes of Health, Bethesda, Maryland, USA, 1997-2009).

S8.   J. Switzer Blum, A. Burns Bindi, J. Buzzelli, J. Stolz, R. Oremland, *Arch Microbiol* **171**, 19 (1998).

S9.   T. Kulp *et al.*, *Appl Environ Microbiol* **72**, 6514 (2006).

S10.   R. S. Oremland *et al.*, *Geochim Cosmochim Acta* **64**, 3073 (2000).

S11.   T. Z. DeSantis, P. Hugenholtz, K. Keller, E. L. Brodie, N. Larsen, Y. M. Piceno, R. Phan, and G. L. Andersen, *Nucleic Acids Res* **34**, W394 (2006).

S12.   T. Z. DeSantis, P. Hugenholtz, N. Larsen, M. Rojas, E. L. Brodie, K. Keller, T. Huber, D. Dalevi, P. Hu, and G. L. Andersen, *Appl Environ Microbiol* **72**, 5069 (2006).

S13.   T. Huber, G. Faulkner, P. Hugenholtz, *Bioinformatics* **20**, 2317 (2004).

S14.   Q. Wang, G. M. Garrity, J. M. Tiedje, and J. R. Cole, *Appl Environ Microbiol* **73**, 5261 (2007).

S15.   T. Hall, *Nucleic Acids Symposium Series* **71**, 95 (1999).

S16.   S. Guindon, O. Gascuel, *Syst Biol* **52**, 696 (2003).

S17.   M.D. Patey, M.J.A. Rijkenberg, P.J. Statham, M.C. Stinchcombe, E.P. Achterberg, and M. Mowlem, *Trends in Anal Chem* **27**, 169 (2008).

S18.   R.G. Wilson, F.A. Stevie, C.W. Magee, *Secondary Ion Mass Spectrometry - A practical handbook for depth profiling and bulk impurity analysis.* (John Wiley & Sons, New York, 1989)

S19.   S.M. Webb, *Phys. Scripta.* **T115**, 1011 (2005).

S20.   M. Newville, *J. Synchrotron Rad.* **8**, 332 (2001).

S21.   J.J. Rehr, S.I. Zabinsky, R.C. Albers, *Phys. Rev. Lett.* **69**, 3397 (1992).

S22.   H. M. Berman *et al.*, *Nucleic Acids Res* **28**, 235 (2000).